Can the Deforestation Breeze Change the Rainfall in Amazonia? A Case Study for the BR-163 Highway Region

Sandra I. Saad,* Humberto R. da Rocha, Maria A. F. Silva Dias, and Rafael Rosolem

Department of Atmospheric Science, Institute of Astronomy, Geophysics and Atmospheric Sciences (IAG), University of São Paulo, São Paulo, Brazil

Received 21 April 2010; accepted 19 July 2010

ABSTRACT: The authors simulated the effects of Amazonian mesoscale deforestation in the boundary layer and in rainfall with the Brazilian Regional Atmospheric Modeling System (BRAMS) model. They found that both the area and shape (with respect to wind incidence) of deforestation and the soil moisture status contributed to the state of the atmosphere during the time scale of several weeks, with distinguishable patterns of temperature, humidity, and rainfall. Deforestation resulted in the development of a three-dimensional thermal cell, the so-called deforestation breeze, slightly shifted downwind to large-scale circulation. The boundary layer was warmer and drier above 1000-m height and was slightly wetter up to 2000-m height. Soil wetness affected the circulation energetics proportionally to the soil dryness (for soil wetness below ~0.6). The shape of the deforestation controlled the impact on rainfall. The horizontal strips lined up with the prevailing wind showed a dominant increase in rainfall, significant up to about 60 000 km^2. On the other hand, in the patches aligned in the opposite direction (north–south), there was both increase and decrease in precipitation in two distinct regions, as a result of clearly separated

* Corresponding author address: Sandra Isay Saad, Rua do Matão 1226, Cidade Universitária, São Paulo-SP 05508-090, Brazil.

E-mail address: sandraisaad@gmail.com

DOI: 10.1175/2010EI351.1

upward and downward branches, which caused the precipitation to increase for patches up to 15 000 km^2. The authors' estimates for the size of deforestation impacting the rainfall contributed to fill up the low spatial resolution in other previous studies.

KEYWORDS: Amazonian deforestation; Land-use change; Climate change; Thermal cell; BRAMS model

1. Introduction

The Amazon region has been threatened in the last 50 years by continuous deforestation promoted by road construction and fostered by rising demands for timber, beef, and soybeans (Hutyra et al. 2005; Nepstad et al. 2008). Notably, the regions in eastern and southern Amazonia (the arc of deforestation) are under higher pressures (Figure 1), leading to increasing susceptibility to fire and ecosystem collapse.

Deforestation has been usually formed as patches with nonregular shapes along the roads and agricultural frontiers. Previous studies of Amazonian deforestation with general circulation models (spatial resolution greater than 100-km cell size) generally lead to a reduction in basin evapotranspiration and rainfall (Nobre et al. 1991; Werth and Avissar 2002). Those reductions basically depended on the decrease in soil water extraction and the continental convergence of moisture transport. Furthermore, dynamic vegetation global models (DGVMs), driven by global scenarios of changing temperature, rainfall, and change in land use, have suggested that roughly one-third of the Amazon basin may be pushed into a permanent dry climate regime (Oyama and Nobre 2003; Hutyra et al. 2005; Sampaio et al. 2007). Amazonian deforestation may impact rainfall in remote areas and play a major role on the global water cycle (Avissar and Werth 2005).

Simulations of the Amazonian deforestation performed at a much finer resolution (i.e., using ~20–40-km cell size) presented contrasting results. For Baidya Roy and Avissar (Baidya Roy and Avissar 2002), mesoscale circulation increased over deforested areas during the dry season; for Ramos da Silva et al. (Ramos da Silva et al. 2008), regional precipitation over deforested areas decreased; and, for Gandu et al. (Gandu et al. 2004), spatially variable changes in rainfall depended on the presence of river valleys and mountain slopes. Such studies prescribed heterogeneous land-use mosaics, over hundreds of square kilometers, and do not commonly agree on the impacts of deforestation. The question of how rainfall may change over local and mesoscale ($<10^2$ and 10^2–10^5 km^2; D'Almeida et al. 2007) deforestation areas is widely open. Soil water storage, clouds, and aerosols play a substantial role in land–atmosphere coupling in the Amazon, where processes of precipitation show strong seasonal variability and cloud growth and formation influenced by fires (Betts and Silva Dias 2010; Martins et al. 2009). Avissar et al. (Avissar et al. 2002) introduced a conceptual model of boundary layer circulation driven by thermal forest–pasture surface gradients, with a lifting mechanism over the deforestation, referred to as deforestation breeze. They suggested patterns of the effect of mesoscale deforestation on rainfall in the Amazon, whereby the rainfall increases with increasing areas of deforestation, and then, after some unknown threshold, rainfall would decrease with further deforestation. Indeed, thermal gradients in Amazonia are supported by field data that show substantial spatial

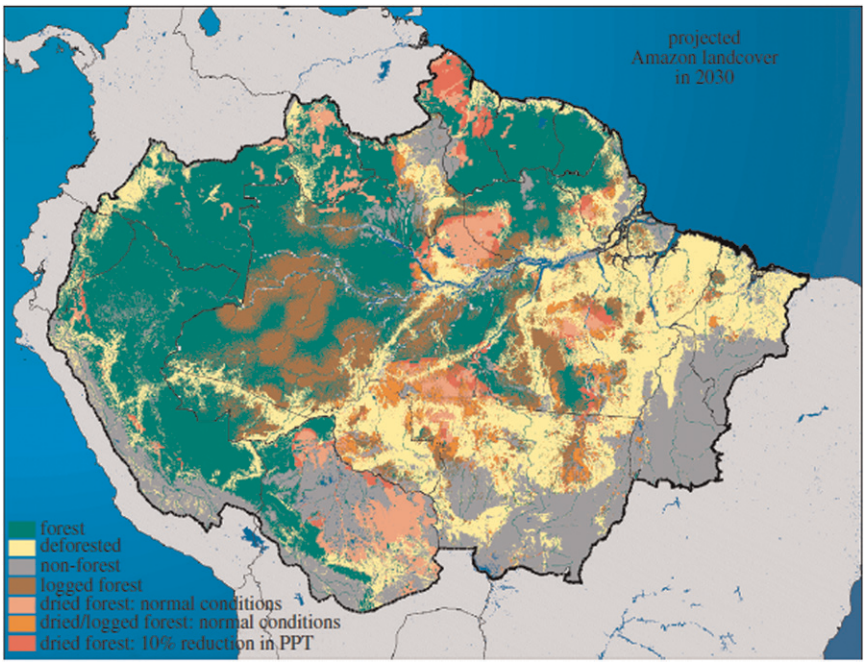

Figure 1. A map of Amazonia 2030 showing drought-damaged, logged, and cleared forests (Nepstad et al. 2008).

changes in latent heat flux varying over bare soil, pasturelands, and tropical humid forests (da Rocha et al. 2009b). However, strong large-scale winds can weaken or advect the modeled instabilities of secondary circulations (Segal et al. 1988; Baidya Roy and Avissar 2002), hence actual changes in rainfall caused by deforestation are uncertain. Analysis is limited to the satellite data showing shallow cumulus cloud development more frequently over grasslands (Cutrim et al. 1995; Wang et al. 2009), probably induced by the deforestation breeze despite its lower potential energy for convection compared to that over the forest. Negri et al. (Negri et al. 2004), however, did detect increased rainfall over deforested areas in the Amazon dry season using satellite estimates.

The state of Pará in the Brazilian Amazonia, which includes the Cuiabá–Santarem Highway (BR-163), a trading corridor near the T juxtaposition of the Amazon and Tapajós Rivers near the city of Santarem, is a region highly affected by deforestation. In the region, the river breeze can control the cloudiness and eventually precipitation especially under weak trade winds (Silva Dias et al. 2004). In addition, Fitzjarrald et al. (Fitzjarrald et al. 2008) reported the near-river stations showed less afternoon convective rain, as would be expected if the river breeze dominates; however, paradoxically, such deficiency was more than compensated for by additional nocturnal rainfall.

This paper aims to explore the modeled changes in rainfall caused by mesoscale deforestation in the region of the Amazonian BR-163 highway over a variable range of patch sizes (varying from 4500 to ~63 000 km^2) and different boundary

conditions, which includes the description of boundary layer processes, control of the soil moisture, river breeze, and the combination of secondary circulation with the synoptic flow.

2. Material and methods

2.1. The BRAMS model

We used the Brazilian Regional Atmospheric Modeling System 3.2 (BRAMS3.2) atmospheric model, built from the sixth version of RAMS (Walko et al. 2000; Cotton et al. 2003) with several new functionalities and parameterizations adapted for tropical and subtropical biomes and soils, using observations or estimations obtained in recent field campaigns in Brazil, mostly associated with the LBA program (Freitas et al. 2009). It uses a set of primitive equations that govern the atmosphere movement and includes prognostic equations for temperature, water vapor, liquid water (for clouds and rain), wind speed, five species of ice crystals, and additional parameterizations of several physical processes (Pielke et al. 1992; Cotton et al. 2003).

For all experiments, the model was set up as follows: 32 vertical layers; horizontally homogeneous initialization of soil moisture with 10 vertical layers; atmospheric initial and boundary conditions of geopotential, temperature, relative humidity, and horizontal speed obtained from the National Centers for Environmental Prediction (NCEP) global model analysis during the year of 2002; topography map from the U.S. Geological Survey (USGS) dataset with 1-km resolution; monthly-mean sea surface temperature field from National Oceanic and Atmospheric Administration (NOAA); radiation transfer from Chen and Cotton (Chen and Cotton 1983); and cumulus parameterization based on Grell and Dévényi (Grell and Dévényi 2002).

The surface–atmosphere exchanges in water, momentum, and energy were calculated with the Land Ecosystem Atmosphere Feedback model (LEAF-3) coupled to BRAMS. Although the model resolution used was no lower than 8 km, the submodel LEAF, coupled to BRAMS, allows multiple surface types to coexist beneath a single grid-resolved column of air. Each surface type or ‘‘patch’’ is able to fractionally weigh several land surface types (e.g., forest, grass, bare soil) (Walko et al. 2000).

Two types of vegetation were prescribed: forest and pasture with original parameters modified after Gash et al. (Gash et al. 1996) and Sakai et al. (Sakai et al. 2004), respectively, namely, emissivity (0.95 for both), vegetation fraction (0.96 for forest and 0.83 for pasture), canopy height (32 m for forest and 0.50 m for pasture), root depth (4 m for forest and 1.1 m for pasture), and roughness length (2.3 m for forest and 0.04 m for pasture). Other parameters were modified as time variant for the months of February, March, April, October, and November: albedo set for forest as 0.122, 0.121, 0.121, 0.135, and 0.135 and for pasture as 0.190, 0.189, 0.188, 0.195, and 0.198, respectively; vegetation leaf area index for forest set as 5.4 m^2 m^{-2} year round and for pasture set as 2.5, 2.2, 1.9, 2.0, and 2.1 m^2 m^{-2}, respectively; and green leaf fraction set for forest as 0.98 year round and for pasture as 0.98, 0.98, 0.98, 0.4, and 0.5, respectively.

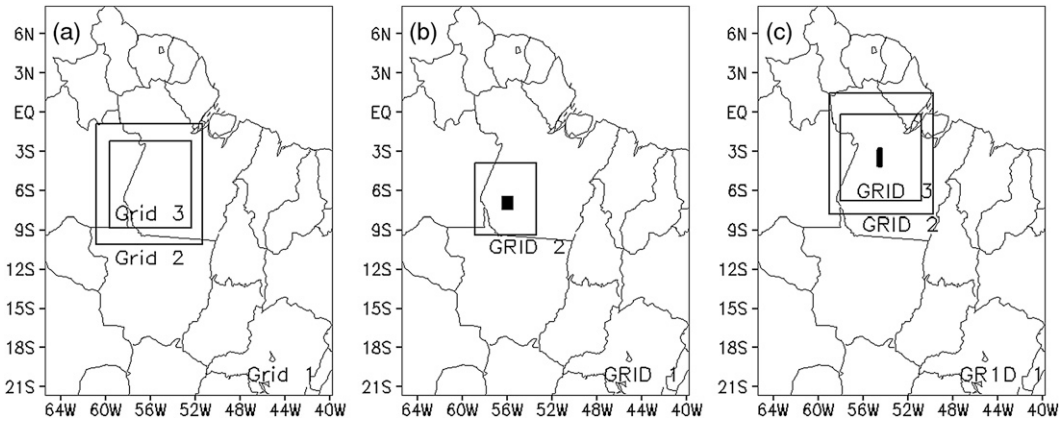

Figure 2. Grid design in the following experimental cases: (a) rainfall case (see the deforestation patch in Figure 3b); (b) soil wetness case (the deforestation patch is the black small rectangle inside grid 2); and (c) river breeze case (the deforestation patch is the black small rectangle inside grid 3).

2.2. Experimental design

We designed three sets of experiments to investigate some control variables associated with the deforestation. For the sake of simplicity, they are called rainfall, soil moisture, and river breeze. In the rainfall case, the size and tilting of a rectangular deforested area were varied, based on the prescription of three nested grids, with size cell resolutions of 64, 16, and 8 km (Figure 2a, Table 1). In the control subexperiment (CTL), forest vegetation was prescribed over the entire domain. In the deforestation subexperiments (DFO) pasture vegetation was prescribed over areas with different rectangular sizes and tilting (Figure 3). The remaining areas were prescribed as forest vegetation, which resulted in eight different cases: AREA1, AREA2, AREA3 and AREA4, all with the longer side of the rectangle aligned in the north–south direction (Figures 3a–d), and AREA1W, AREA2W, AREA3W and AREA4W, with the longer side of the rectangle aligned with the mean surface wind direction, referred to here simply as tilted (with respect to north–south direction) rectangle (Figures 3e–h). Mean wind direction calculated in the CTL case was 64°, or east-northeasterly wind. The rectangular patches of deforestation varied from ~4500 (for both AREA1 and AREA1W) to ~63 000 km^2 (for both AREA4 and AREA4W). The CTL and the eight DFO experiments of the rainfall case were performed both in the dry season (beginning on 1 October) and in the rainy season (beginning on 1 February), and each lasted 61 days (see Table 1). The initial soil moisture was prescribed as horizontally homogeneous and vertically heterogeneous over 10 layers, reaching a maximum depth of 6-m depth (Figure 4) based on data near Santarem (Bruno et al. 2006). The differences between the several DFO experiments and the CTL were calculated as temporal and areal averages constrained by the *t* test at the 95% significance level (Findell et al. 2006), because homogeneous variance was observed.

In the soil moisture case, we investigated the sensitivity of the energy balance partitioning and the boundary layer temperature and moisture to the soil moisture

Table 1. Grid design and experimental conditions used in the BRAMS model, for the three experiments: rainfall, soil moisture, and river breeze. For additional details, see Figure 2.

Grid design and experimental conditions	Rainfall case	Soil moisture case	River breeze case
No. of cells (x, y) in grid 1	40, 50	40, 50	40, 50
No. of cells (x, y) in grid 2	62, 62	38, 38	62, 62
No. of cells (x, y) in grid 3	98, 90	—	98, 90
No. of cells (x, y) in grid 4	—	—	—
Lat and lon of grid 1	7°S, 53°W	7°S, 53°W	7°S, 53°W
Lat and lon of grids 2, 3, and 4	7°S, 56°W	7°S, 56°W	3.5°S, 54.5°W
Grid spacing of grids 1–4 (km)	64, 16, 8	64, 16	64, 16, 8
Vertical coordinate	sigma z	Shaved Eta	sigma z
Period of simulation	1 Oct (dry season) and 1 Feb 2002 (wet season), during 61 days	5 Nov 2002, during 10 days	1 Oct 2002, during 61 days
Topography and resolution	USGS 1 km	USGS 10 km	USGS 1 km
Initial soil moisture profile	Field data	Field data and 18 profiles (dry to wet)	Field data
Simulated cleared area (km^2)	from 4000 to 60 000	100 × 100	50 × 350

initialization. We performed a control experiment prescribed with homogeneous forest vegetation over the domain and initial soil moisture based on field data (solid line in Figure 4, similar to rainfall case). In addition, another 36 experiments were prescribed with different initial soil moisture profiles, which ranged from very dry

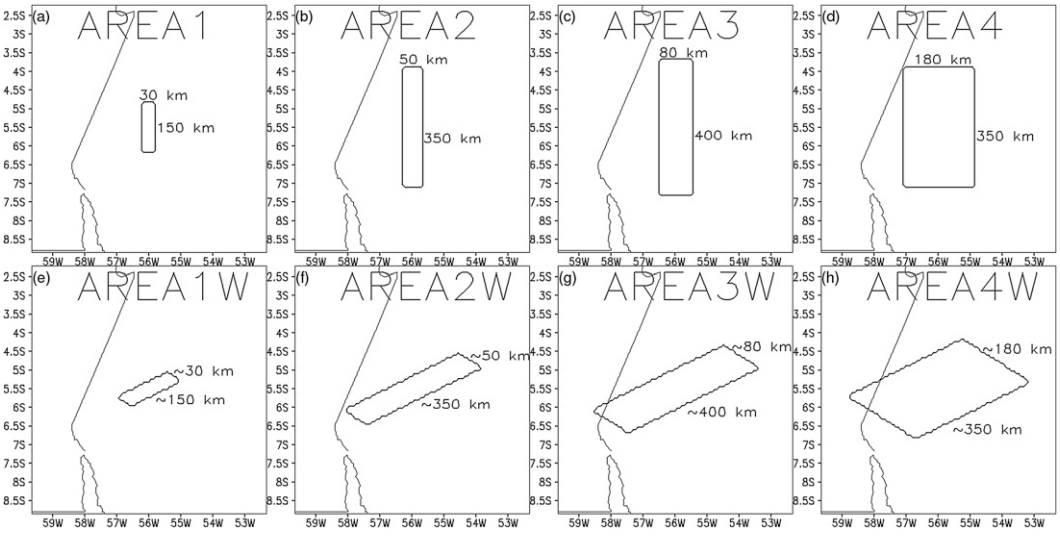

Figure 3. Deforested areas prescribed over the following rectangles (DFO cases): (a)–(d) AREA1–AREA4, aligned the in north–south direction, and (e)–(h) AREA1W–AREA4W, aligned with the prevailing surface wind direction (referred here as tilted patches). The rectangular patches varied from 4500 to about 63 000 km^2.

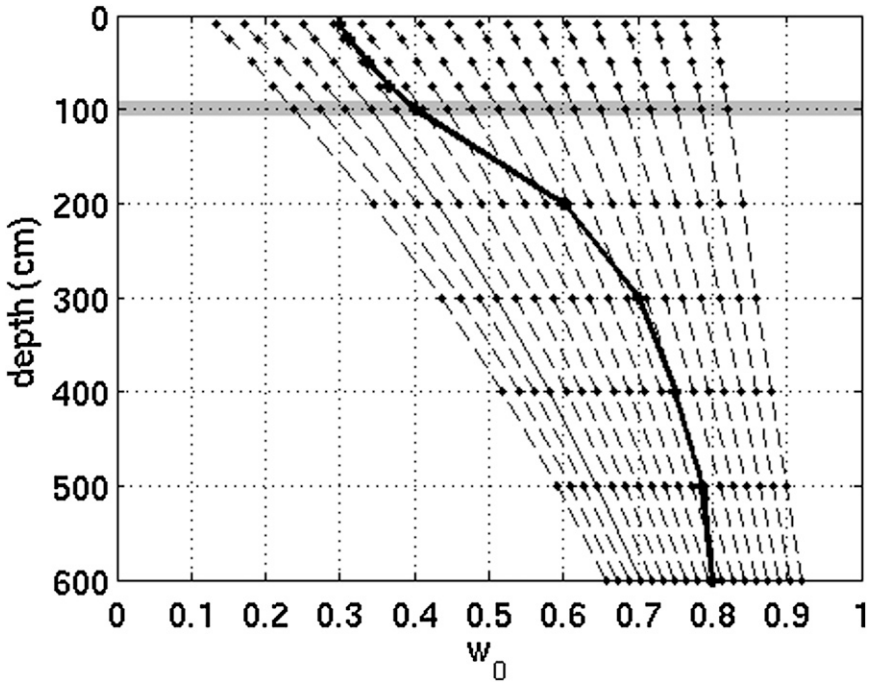

Figure 4. Initial soil wetness of the following experiments: 1) the 37 subexperiments of the soil wetness case (18 dashed lines plus the solid line); 2) rainfall experiment/dry season case and river breeze experiment, which used field observations (solid line); and 3) rainfall experiment/wet season, which used the wettest profile (dashed line). The highlighted height is the pasture root depth (100 cm), mentioned throughout the discussion of soil moisture case results.

to very wet conditions at shallower soil layers (dashed lines in Figure 4), wherein half of them (18 experiments) prescribed forest vegetation in the entire domain and the remaining half prescribed deforested areas of 100 km × 100 km (Figure 2b, Table 1). All 37 experiments of the soil moisture case used two nested grids with 64- and 16-km resolution, respectively, and were simulated during a period of 10 days starting on 5 November.

In the river breeze case, we attempted to test how the modeled Amazon–Tapajós river breeze may compose the circulation generated by the deforestation patches. This case used three grids (Figure 2c, Table 1) similar to those of the rainfall case and carried out four different experiments: 1) forest vegetation prescribed over the whole domain (CTL; Figure 5a); 2) the previous CTL setup with an additional river network (RIV; i.e., forest and rivers; Figure 5b); 3) with the previous CTL setup with additional deforestation over a 50 km × 350 km area (DFO; i.e., forest and deforestation; Figure 5c); and 4) with the previous CTL experiment with additional deforestation and river network (DFORIV; i.e., forest, deforestation, and rivers; Figure 5d). All these four experiments were initialized on 1 October and simulated for a period of 61 days. Soil moisture was initialized similarly as in the rainfall case (Figure 4).

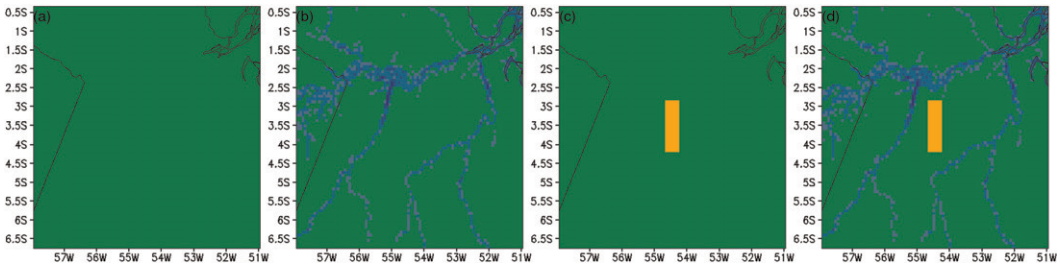

Figure 5. Land surfaces used in river breeze case for: (a) CTL, (b) RIV, (c) DFO, and (d) DFORIV. The green, blue, and orange colors represent the forest, water bodies, and pastureland, respectively.

3. Results and discussion

3.1. Rainfall case

The 10-m wind was higher for a simulation in the dry season (~3 m s^{-1}) than for a simulation in the rainy season (~2 m s^{-1}; Figure 6). The predominant direction was from east-northeast or, more precisely, 64° in the dry season, which compared well with the regional climatological circulation. The calculated latent heat flux in the CTL cases for the forest vegetation during both the dry and rainy season overestimated the field data over a tropical forest near Santarem (da Rocha et al. 2004; da Rocha et al. 2009a) by about 50%. This was a consequence of a similar overestimation magnitude in the calculated net radiation and an overestimation of incoming solar radiation of about 40%. The modeled surface solar irradiance seemed systematically high and possibly associated with simulated lower cloud cover fraction.

Figures 7–10 show the mean difference (DFO − CTL) of sensible heat flux H and of the latent heat flux LE in the dry and rainy seasons for the 61-day simulations of grid 3. In the dry season, the increase in H (Figure 7) in the DFO case, decrease in LE (Figure 9) and, consequently, the increase in Bowen ratio (not shown) were generally stronger upwind (eastern sectors), with also some increase in the southern face of the tilted patches (Figures 7, 9e–h). The mean areal changes in H in the dry season were between 23 and 26 W m^{-2} (Figure 7), about twice of those in the wet season, which were between 10 and 12 W m^{-2} (Figure 8). The mean difference (DFO − CTL) of latent heat flux LE showed a decrease of between 38 and 48 W m^{-2} in the DFO experiment during the dry season (Figure 9). In the rainy season, however, the differences of LE were very small (Figure 10). The DFO case in the dry season showed an increase in the mean canopy air temperature of 0.6°C, a decrease in mean canopy specific humidity of 0.4 g kg^{-1}, and an increase in the mean canopy wind speed of 0.3 m s^{-1} (not shown).

The mean difference of precipitation (DFO − CTL) in the dry season (at the 5% significance level, in Figure 11) showed increasing (decreasing) precipitation for the DFO experiment near the upwind (downwind) edges of the deforestation patch, which also coincided with the sectors just upwind and downwind where the fluxes H and LE mostly varied. Thus, rainfall appeared to increase downwind and, conversely, decrease upwind in the deforestation area, which can be explained by the

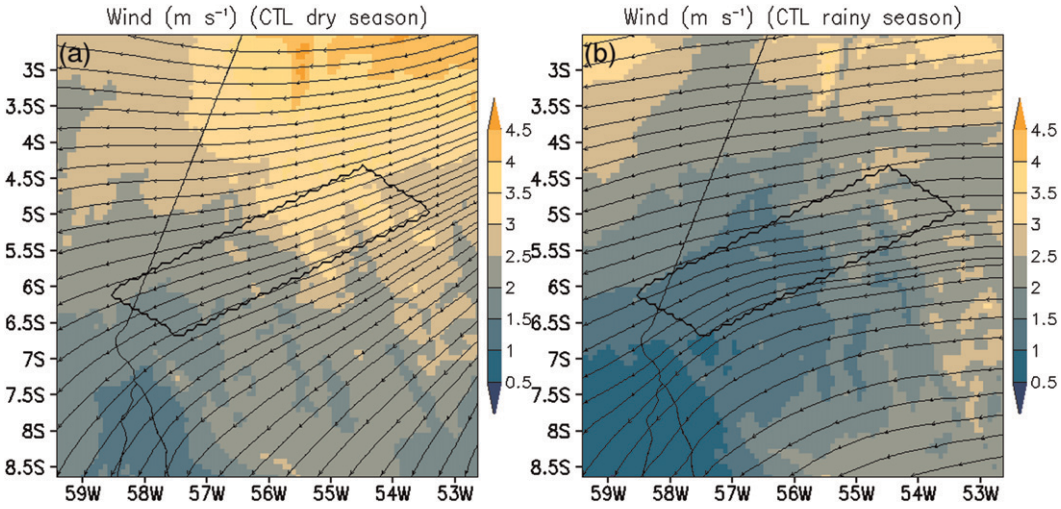

Figure 6. Mean horizontal wind speed/magnitude (at 400-m height) for the CTL case in the (a) dry season and (b) rainy season. The rectangle shows the deforestation area (AREA2W), which suggests how the wind direction coincides with the longer side of the rectangle.

horizontal transport of both mass and humidity downwind (east-northeasterly), along with a deforestation breeze type of circulation, which is now discussed.

Especially in most of the tilted patch experiments (Figure 11e–h), we observed a higher increase in precipitation downwind relative to the decrease upwind in comparison to the nontilted experiments (Figures 11a–d). That is, a more pronounced areal imbalance of increasing/decreasing precipitation was noticed over the tilted patches. For example, in the AREA2W experiment (Figure 11f), rainfall increased (decreased) by 49 mm (−23 mm), with a net increase of 26 mm. In comparison, in the equivalent experiment AREA2 (Figure 11b), rainfall increased (decreased) by 40 mm (−43 mm) and with a net change of only −2 mm. On the other hand, the surface areas with significant rainfall changes were generally less pronounced in the tilted patch experiments. For example, AREA2W showed 139 impacted cells (colored pixels, Figure 11f), whereas the AREA2 experiment showed 397 impacted cells (colored pixels, Figure 11b). For the latter, the sectors with either increase or decrease in precipitation appeared to be in two quite distinct positions, as a result of two clearly separated upward and downward branches.

The changes in rainfall were generally more horizontally spread over the tilted patches in comparison to the nontilted patches. Overall, the nontilted patch experiments showed only small net changes in precipitation (+7%, −2%, −7%, and −5% for AREA1–AREA4, respectively; Figures 11a–d). In contrast, the tilted patch experiments tended to show more substantial net precipitation (+22%, +14%, +12%, and −2% for AREA1W–AREA4W, respectively; Figures 11e–h), which in turn also favored a net increase in precipitation (positive changes) concurrent with more reduced deforested patches. The effect of the wind incidence was less dramatic in the largest patch, because the boundaries with wind input have similar lengths in both tilt and nontilt rectangles (Figures 11d,h, respectively).

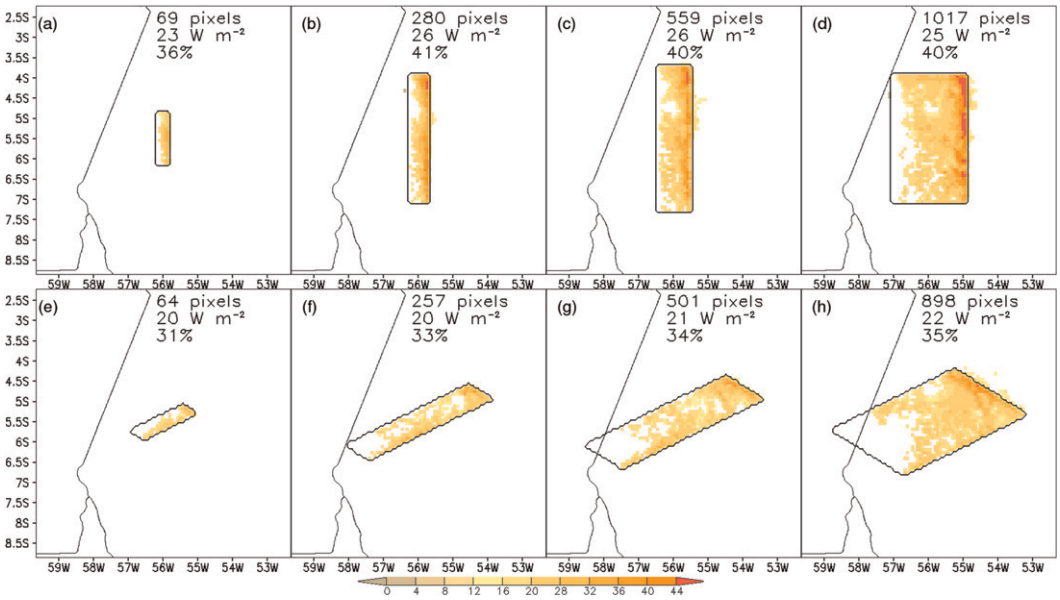

Figure 7. (a)–(h) Difference (DFO − CTL) of the mean sensible heat flux (in W m^{-2}) for each deforestation patch in the dry season period. The values shown are number of cells, mean areal difference in sensible heat flux (in W m^{-2}), and mean percentage increase/decrease in DFO case compared to CTL. The differences were all with the 5% significance level.

The spatial patterns with exclusive areas of increasing and decreasing precipitation appeared to be similar in the wet season (Figure 12) but showed a reduction in both the areal extension and the net precipitation relative to the dry season. For example, in the AREA2 experiment, the percentage of impacted area with increasing (decreasing) precipitation in the DFO experiment was +21% (−22%) in the dry season and +13% (−15%) in the rainy season. These seasonal changes were likely driven mostly by the decrease in sensible heat flux differences in the rainy season and driven partly by the decrease in wind magnitude, which disfavors mechanical mixing. The weakening of the changes in precipitation during the rainy season in Amazonia deforestation has been reported by other authors (Gandu et al. 2004). Furthermore, changes in precipitation were greater over the nontilted patches (Figures 12a–d) in comparison to the tilted patches (Figures 12e–h), which is partially explained by the influence of the crosswind (northerly component in the example of the nontilted patches) intensifying the deforestation breeze by lateral mass convergence.

The changes in precipitation were concurrent with the development of thermal cells in the boundary layer, with upward motion driven by the warm core over the deforested area and compensatory lateral downward motion. For example, in the AREA2 and AREA2W experiments during the dry season, we noticed areas of varying temperature with changes of approximately +1.5 K over the cleared surface, +0.5 K at 1000-m height, and with slight cooling of −0.1 K above 3000-m height (Figure 13). In addition, specific humidity was reduced from about −0.5 to −1.5 g kg^{-1} in the surface layer up to about 500-m height and was slightly

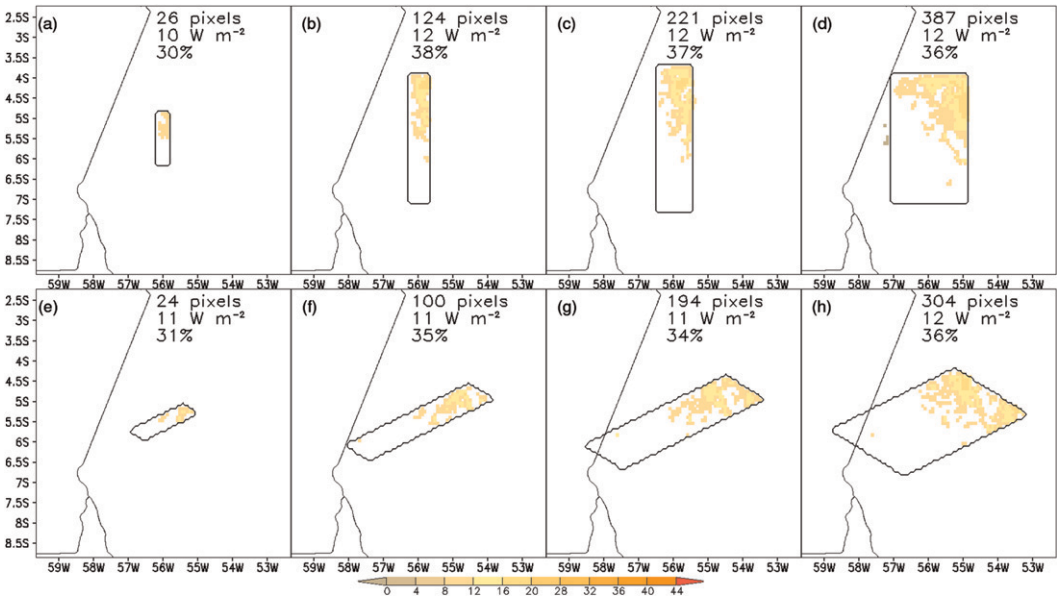

Figure 8. As in Figure 7, but for the rainy season period.

greater over the cleared area from about 500- to 3000-m height. The dryness in the lower layer was caused by lower evapotranspiration from pastureland, which contributed to dry up the shallower soil layers. The higher humidity in the upper layer was a consequence of the horizontally transported humid air from the forest followed by upward motion, carrying lower wetter air, which moistened the upper

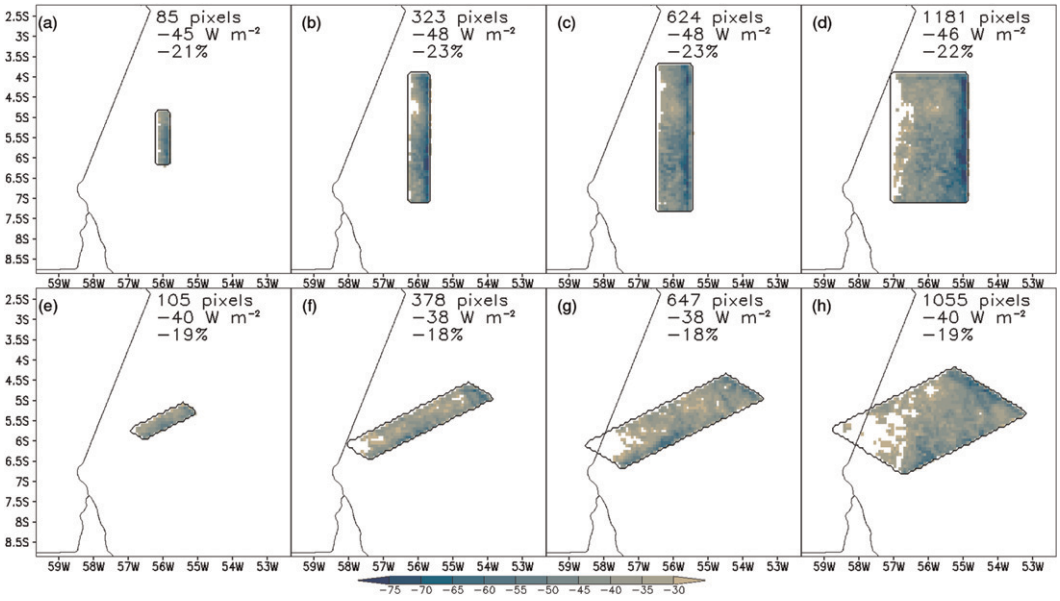

Figure 9. As in Figure 7, but for the latent heat flux LE (in W m^{-2}).

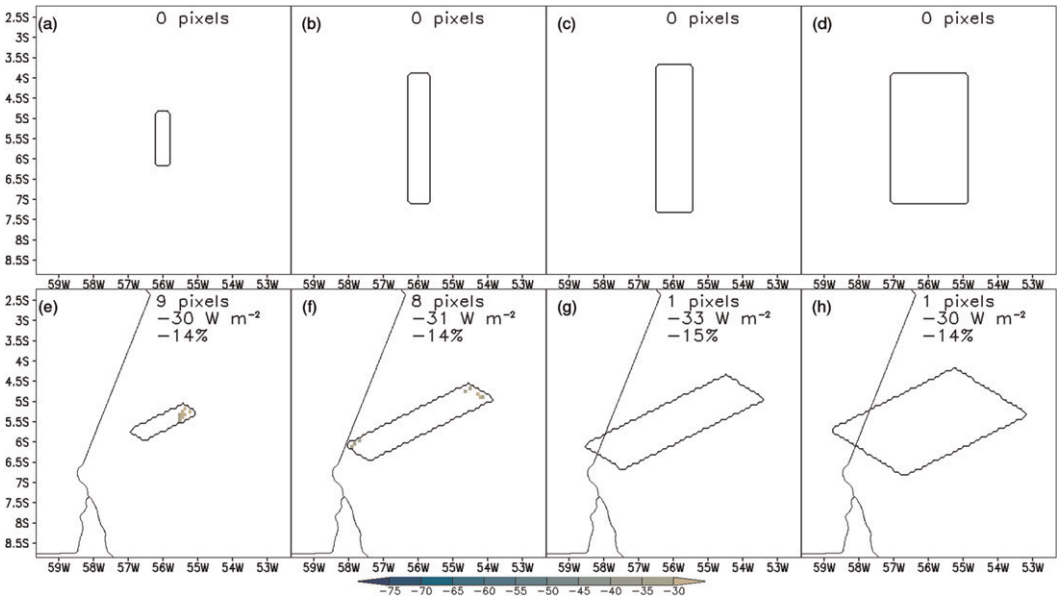

Figure 10. As in Figure 7, but for the latent heat flux LE (in W m^{-2}) during the rainy season period.

layers. The pattern of modeled warm boundary layer compares well with field observations of warmer convective boundary layer over deforested areas in Amazonia and lower surface humidity (Nobre et al. 1996; Fisch et al. 2004). We have not found any references reporting changes in the upper boundary layer humidity to compare with our modeled results.

The atmospheric circulation showed a mass convergence zone downwind and near the edge of the cleared patch (Figure 13a), with an apparent thermal cell shifted westward in the prevailing wind direction. Interestingly, the circulation showed a dominant horizontal upper branch with eastward wind and downward motion near the east edge of the clearance, which helps to explain why precipitation decreased only eastward or upwind from the clearance. Changes in temperature, humidity, and wind in experiments AREA1, AREA3, and AREA4 were similar to AREA2 (not shown) with a small exception for AREA4, where the convergence mass zone was relatively larger than the others. In the north–south direction, however, we noticed in the AREA2 experiment the existence of two upper horizontal wind branches on both the northern and southern edges of the clearance (Figure 13b). Also, the vertical changes in boundary layer humidity were similar to those noticed in the east–west section (Figure 13a) and were mostly evident south of the clearance.

The circulation in the cross section positioned approximately incident to the prevailing wind (i.e., the AREA2W experiment; Figure 13c) showed both a convergence zone and upward motion centered over the clearance, with two upper lateral branches at approximately 2000 m. The changes in the vertical boundary layer profile of temperature and humidity were almost similar to the AREA2 experiment. Such a circulation pattern was under very little influence of the prevailing

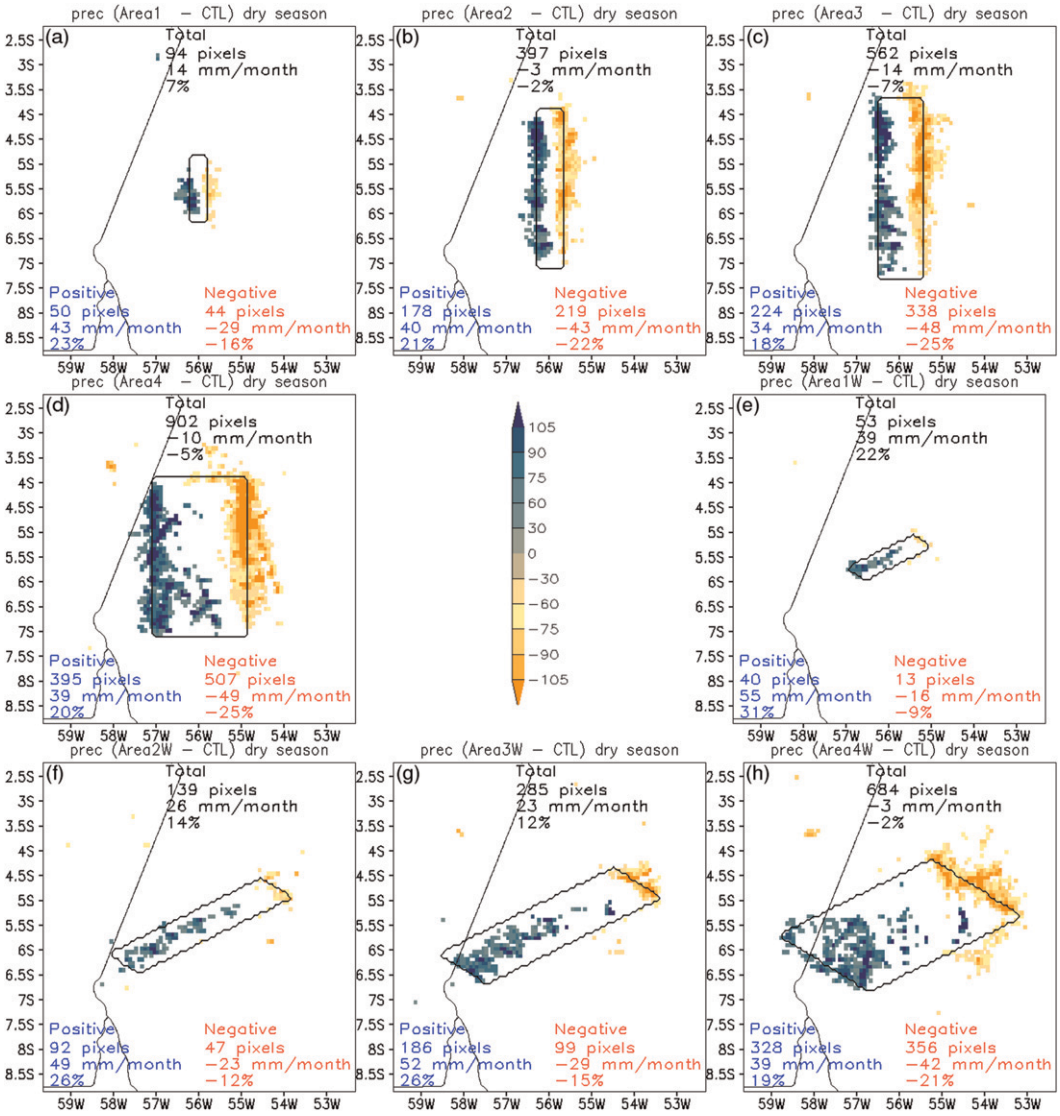

Figure 11. Mean difference (DFO − CTL) precipitation simulated in the dry season (at the 5% significance level); increasing (decreasing) precipitation in the DFO experiment shown as blue (yellow) color shading) for all experiments shown in Figure 3. The values shown in black at the top are number of cells with significant changes in precipitation, mean precipitation change over significant cells (in mm month^{-1}), and percentage change of precipitation (DFO − CTL). The values shown in blue at the bottom right are as in the top, but for the cells where precipitation increased in the DFO experiment. The values shown in red at the bottom right are as in the top, but for the cells where precipitation decreased in the DFO experiment.

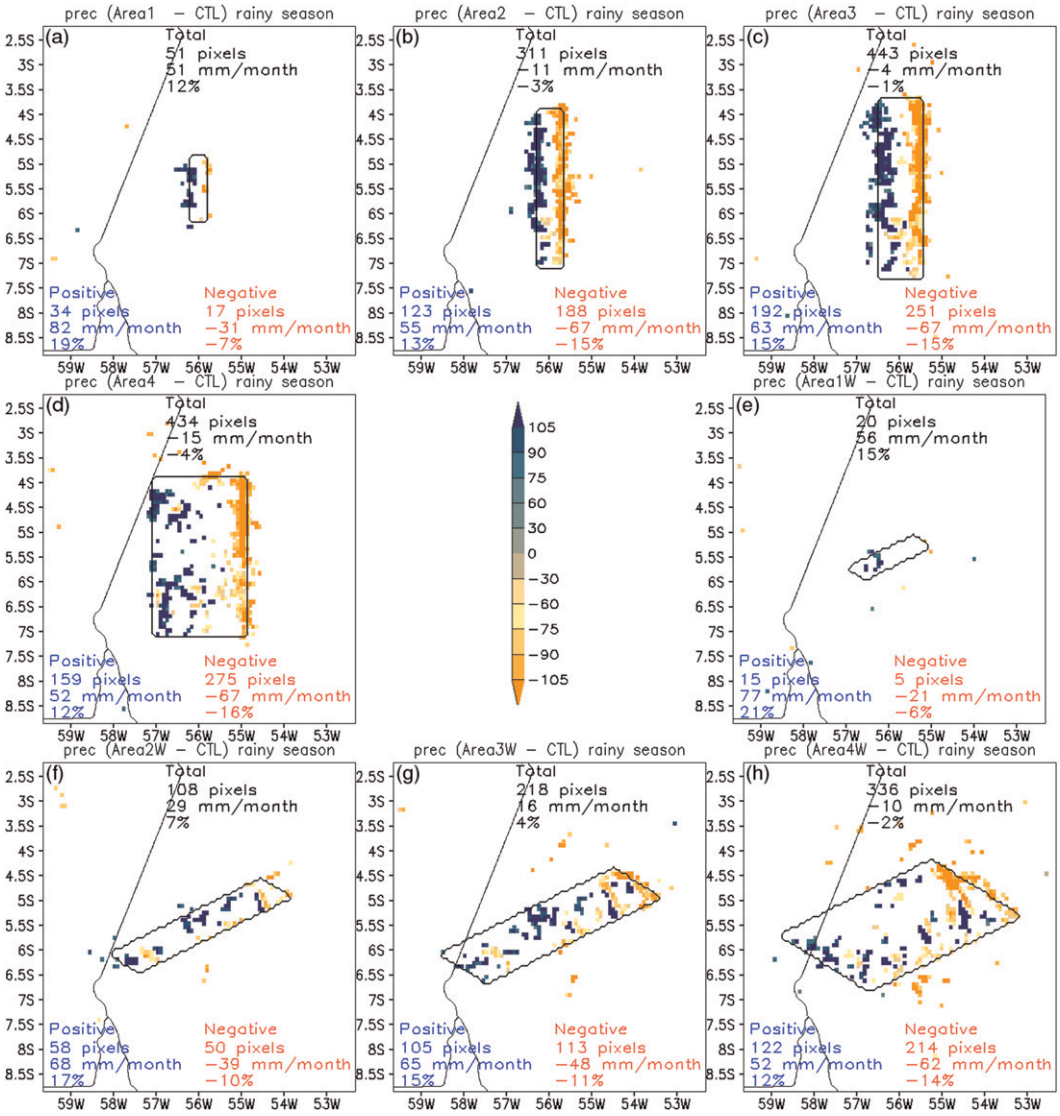

Figure 12. As in Figure 11, but for the simulation in the rainy period.

wind, because the patch area and wind are nearly perpendicular to each other and mostly resemble the simple and idealized concept of the two-branch thermal cell. Downward lateral branches are not observed (only values above 0.3 m s^{-1} are shown) although the surface convergence is a consequence of their effect. Interestingly, a likely expected impact of the descending lateral motion to suppress rainfall outside the convergence zone was not observed here, presumably explained by the effect of weak circulation with little or no contribution to the prevailing wind. A similar result is observed in Figure 13b, which shows no rainfall suppression north or south of the clearance.

In the AREA2W experiment, with the cross section lined up with prevailing wind (Figure 13d), a strong ascendant branch appeared to completely dominate the

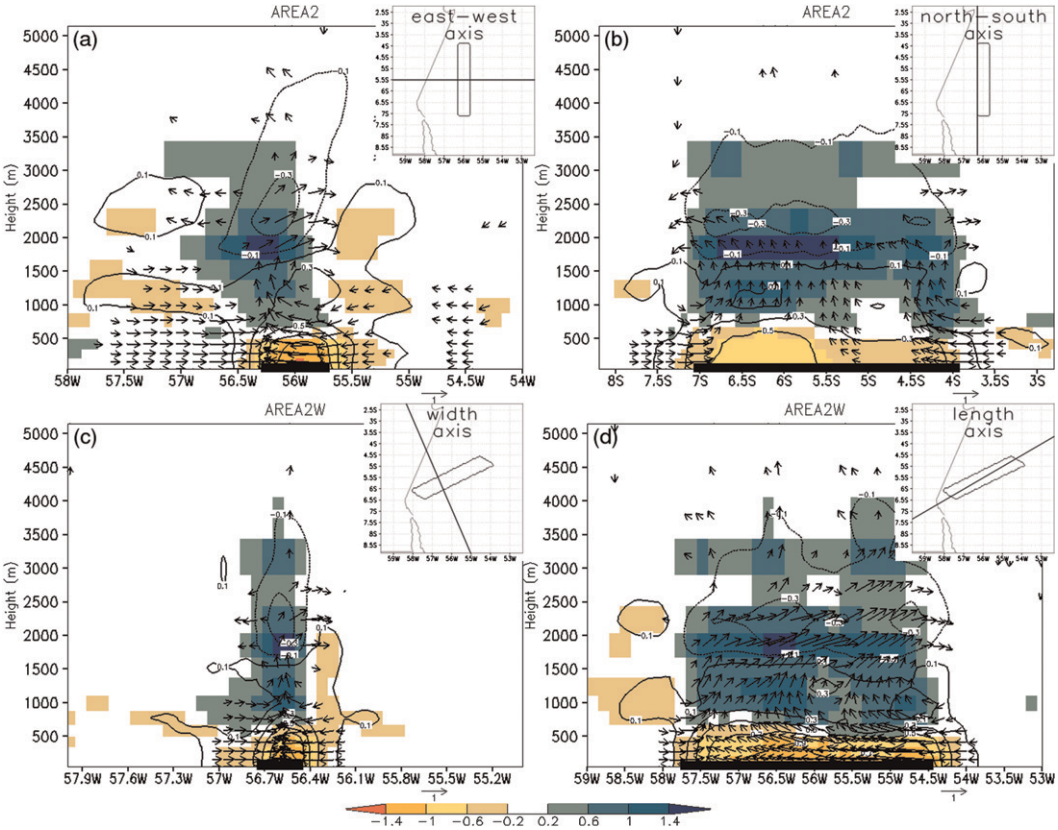

Figure 13. Vertical cross sections (height vs latitude or longitude) of the difference (DFO − CTL experiments) wind (vectors; in m s^{-1}; only values > 0.3 m s^{-1} are shown), specific humidity (shaded color; in g kg^{-1}), and potential temperature (contour line; in °C) (a) in the east–west axis in the AREA2 experiment, (b) in the north–south axis in the AREA2 experiment, (c) in the rectangle's width parallel axis in the AREA2W experiment, and (d) in the rectangle's length parallel axis in the AREA2 experiment. The black horizontal bar in abscissa shows the cleared areas. The inset in each plot highlights the direction of the cross section with respect to the deforestation area of interest.

clearance and lead to distributing the area of increase precipitation more uniformly (Figure 11f). Notwithstanding, the AREA2 and AREA2W experiments both had similar responses, with the enhancement of a counter–vortex flow, against the prevailing wind, though allowing for asymmetry of the secondary circulation, which helped to reduce the precipitation just upwind of the edges of the clearance. It is suggested that the incidence of the wind over lower surface roughness areas in the clearance edge leads to increase in acceleration, which in turn resulted in downward movement for mass compensation and ultimately strengthened the counter–vortex flow.

Figure 14 summarizes our results in terms of percentage difference of rainfall as a function of deforested area. In general, the magnitude of changes is greater for

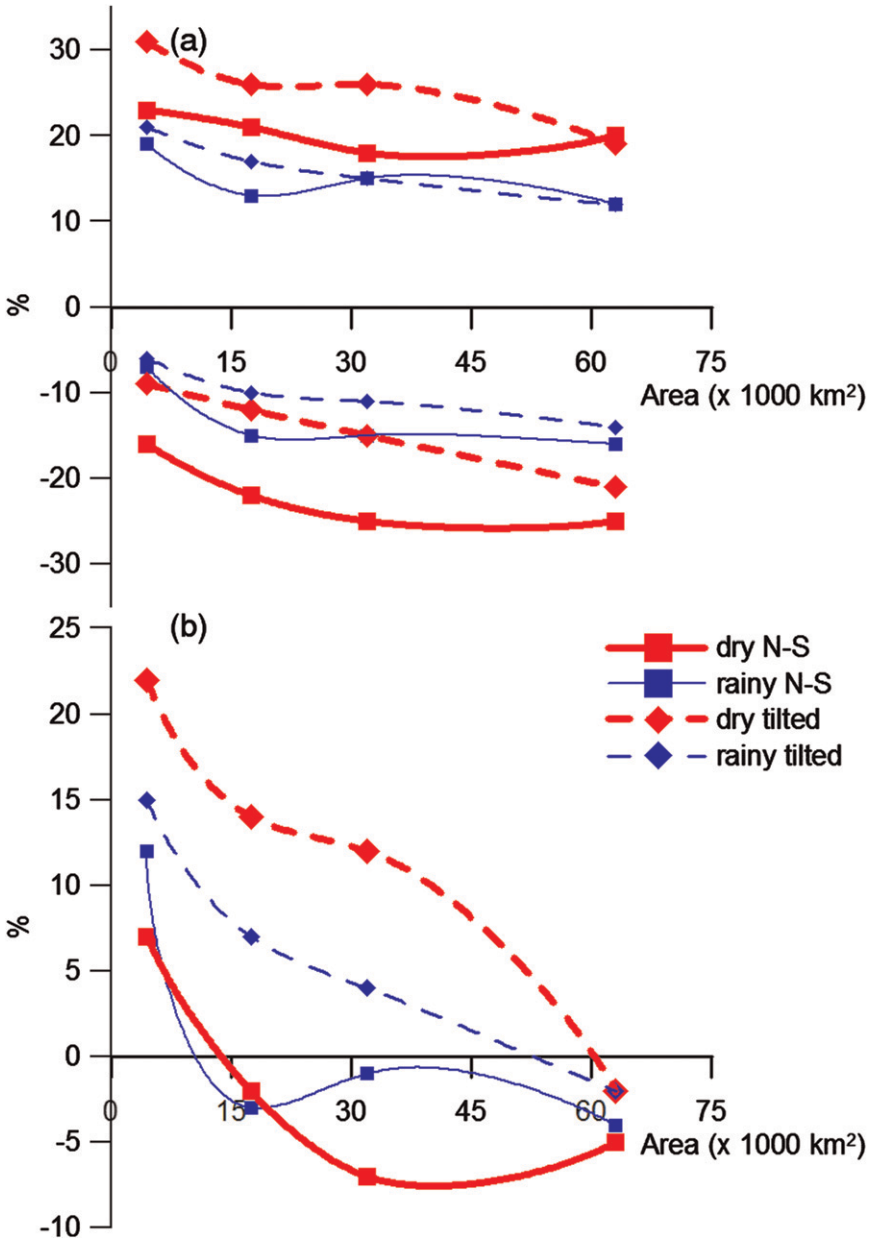

Figure 14. Percentage difference in rainfall as a function of deforested area for (a) the zones where the rainfall increased (lines with positive values) and the zones where the rainfall decreased (lines with negative values) and for (b) the entire deforested area.

small deforested areas for the areas where rainfall increases (positive values in Figure 14a); in contrast, the magnitude of changes increases as the deforestation area increases for the areas where rainfall is reduced (negative values in Figure 14a). The net change in precipitation (Figure 14b) shows a clear distinction between the north–south-oriented and the tilted patches: it is seen that the change

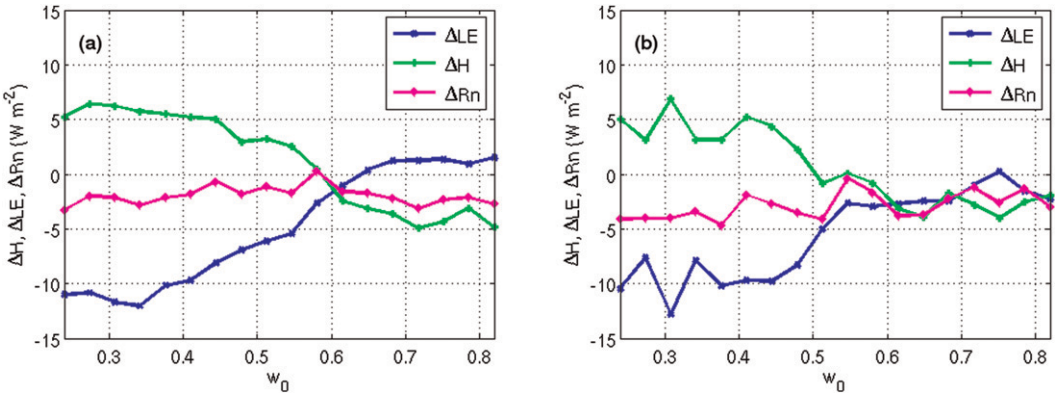

Figure 15. Mean temporal and areal (over the clearance area) difference (DFO − CTL experiment) of sensible heat flux ΔH, latent heat flux ΔLE, and net radiation ΔRn (all in W m^{-2}) with varying initial mean soil wetness down to 1-m depth w_0 for (a) w_0 over the forest patch only, prescribed as in Bruno et al. (Bruno et al. 2006), for both the CTL and the remaining 18 DFO experiments and (b) w_0 prescribed variable for both forest and pasture patches as in the 18 soil wetness profiles (see Figure 4).

from increase to decrease in rainfall occurs for an area of 15 000 km^2 for the former, whereas this threshold is around 50 000 km^2 for the tilted patches. Notice that at 50 000 km^2 the magnitude of changes in precipitation for all cases tends to coincide (about 5% reduction in rainfall). The implications of these results on the possible overall effect of actual deforestation patches in the Amazon on rainfall suggest some additional information to the patterns suggested by Avissar et al. (Avissar et al. 2002), as mentioned above.

3.2. Soil moisture case

The mean temporal and areal differences (DFO − CTL experiment) of sensible heat flux ΔH, latent heat flux ΔLE, and net radiation ΔRn calculated over the cleared area with varying initial soil wetness w_0 are shown in Figure 15a. We noticed that H increased and LE decreased in the DFO experiment, for a range of soil wetness between about 0.2 and 0.6 at 100-cm height. This result is similar to that obtained in the rainfall case, because the changes in the energy fluxes were weaker for wetter soils (Figures 8, 10). For w_0 greater than 0.60 (Figure 15a), there was a slight increase in LE and decrease in H. In addition, the net radiation was generally less in the DFO experiment and remained nearly steady, with varying wetness.

The initial soil moisture was prescribed as constant under the forest patch only (Figure 4) for both the CTL and the remaining 18 DFO experiments shown in Figure 15a. In addition, we prescribed initial soil moisture in 18 other experiments varying progressively over both forest and pasture patches, which likewise showed a reduction in LE in the DFO experiment over the entire soil moisture range (Figure 15b) and also a variation of H and Rn similar to that shown in Figure 15a. In all

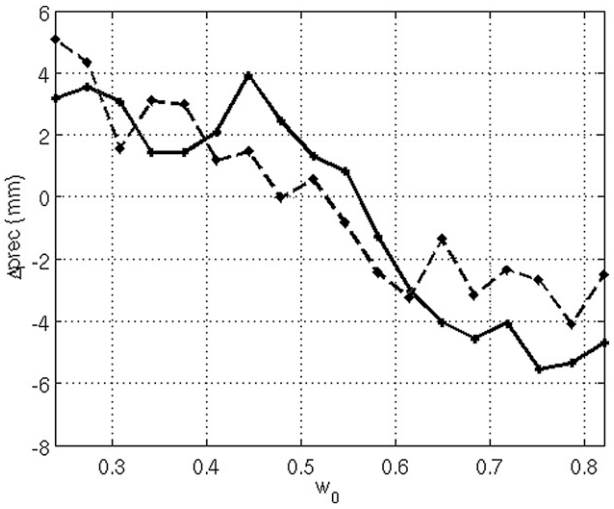

Figure 16. Mean difference (DFO–CTL) of accumulated precipitation in 10 days (in mm) with varying initial soil wetness w_0, calculated over the area 7.7°–6.5°S, 56.7°–55.5°W. The solid line is the case with w_0 over the forest patch only prescribed as in Bruno et al. (Bruno et al. 2006; see Figure 4) for both the CTL and the remaining 18 DFO experiments; the broken line is the case with w_0 prescribed as variable for both forest and pasture patches as in the 18 soil wetness profiles (see Figure 4).

experiments, however, changes in LE were systematically higher with soil dryness conditions and tended to approach zero at about 0.65 and 0.75 initial soil wetness. This threshold agrees quite well with the simulated conditions using the Simple Biosphere Model (SiB) calibrated for two pasture sites in Amazonia ($w_0 = 0.6$; da Rocha et al. 1996).

The mean areal difference (DFO − CTL) in precipitation (Figure 16) was calculated over the area with maximum precipitation within the domain approximately coincident with the area of increasing precipitation shown in Figure 11. We noticed that deforestation caused an increase in precipitation mainly when the soil is very dry ($w_0 = 0.2$; Figure 16). No difference in precipitation is observed when $w_0 \sim 0.55$; beyond this threshold, less precipitation is observed in the deforestation experiment relative to the control experiment up to the wettest soil status ($w_0 = 0.85$). The increase in precipitation driven by deforestation with low soil moisture status compares well to our experiments in the rainfall case, because the dry season (drier soil) showed greater impact on rainfall.

Furthermore, changes in the boundary layer are shown in Figure 17 as a cross section of the mean difference (DFO − CTL) experiments of specific humidity and potential temperature with varying soil wetness. For the drier soil status ($w_0 < 0.6$), the DFO boundary layer appeared to be warmer (Figure 17b) and drier in the lower layers up to about 800-m height; on the other hand, it appeared to be wetter approximately from 1000- to 2000-m height (Figure 17a). These changes looked similar to those discussed in the rainfall case (Figure 13). For wetter soils ($w_0 >$ 0.6), changes in temperature were not observed (Figure 13b). However, humidity

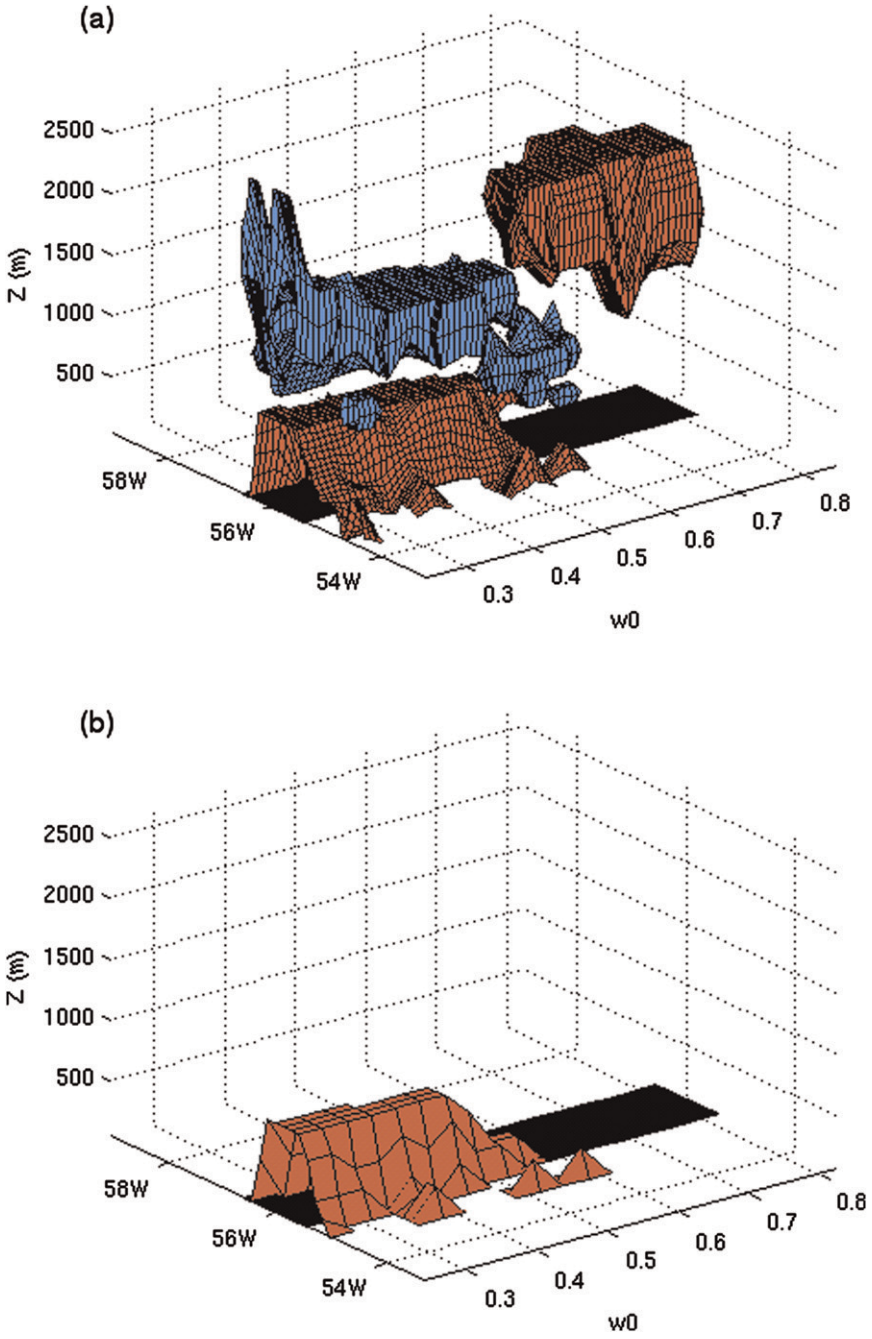

Figure 17. Cross section, at 6.9°S, of the mean difference DFO − CTL with varying initial soil wetness w_0 for (a) specific humidity with contours of +0.2 g kg^{-1} (in blue; i.e., wetter in DFO) and −0.2 g kg^{-1} (in red; i.e., drier in DFO) and (b) potential temperature with contours at +0.2 K (in red; i.e., warmer in DFO). The black horizontal strip at Z = 0 shows the cleared area.

decreased in the upper boundary layer, approximately above 1500-m height (Figure 13a), which was possibly due to the decrease in evapotranspiration over the cleared area.

3.3. River breeze case

Mean differences of precipitation from RIV − CTL, DFORIV − DFO, DFO − CTL, and DFORIV − RIV are shown in Figure 18 for changes in the accumulated 24-h precipitation, daytime and nighttime only, respectively. First, we noticed that changes in precipitation were greater during the daytime (center panels in Figure 18) compared to the nighttime (right panels in Figure 18). For example, precipitation increased downwind from the cleared area and decreased upwind in the DFO − CTL experiment mainly during the daytime (Figure 18h). In comparison, during the nighttime, there were only small changes in precipitation over and around the cleared area (Figure 18i). The overall result of DFO − CTL seems to agree with the previous discussion of the rainfall case.

Second, the inclusion of the water bodies in the domain of simulation remarkably decreased the precipitation over the river network (RIV − CTL; Figures 18a–c) caused by mechanisms of the modeled river breeze circulation. In addition, the precipitation increased over certain areas around the rivers, which included the northern sector of the cleared area, especially during the daytime (Figure 18b). For the nocturnal period, one would expect to see the opposite effect of the day because of the land breeze, as observed by Fitzjarrald et al. (Fitzjarrald et al. 2008), who noticed a substantial increase in nighttime precipitation close to the rivers. On the contrary, precipitation also decreased in Amazonian rivers during the nocturnal period (Figure 18c), although with less intensity than in the day (Figure 18c). Probably, the effect of land breeze would be noticed if a period lower than 12 h had been considered for the averages.

However, the differences RIV − CTL were comparable to DFORIV − DFO (Figures 18d–f); in addition, DFORIV − RIV (Figures 18d–f) appeared to be similar to DFO − CTL (Figures 18g–i). In summary, this suggests that the presence of the river network did not change our interpretation of the effects of deforestation on the rainfall and soil moisture cases. More precisely, the calculation of the mean difference (DFORIV − RIV) − (DFO − CTL) (Figure 19) based on the Stein–Alpert analysis (Pielke 2002), which represents the interaction between pairs of changes when two changes in the control simulation are prescribed for the same study, did not show changes similar to those with the separated effect of deforestation. It helps to support the hypothesis that the clearance was prescribed sufficiently far from the rivers so as not to be strongly affected by their circulation.

4. Conclusions

We simulated the effects of deforestation in the boundary layer and in the rainfall for a region in eastern Amazonia near the Tapajós River using the BRAMS model and discussed the structure and impacts of the deforestation breeze. Scenarios of pasturelands were prescribed as rectangles with varying size, soil wetness, and wind incidence. The circulations driven by river breeze did not affect the circulations driven by a deforestation breeze. Our findings showed that, in general, both

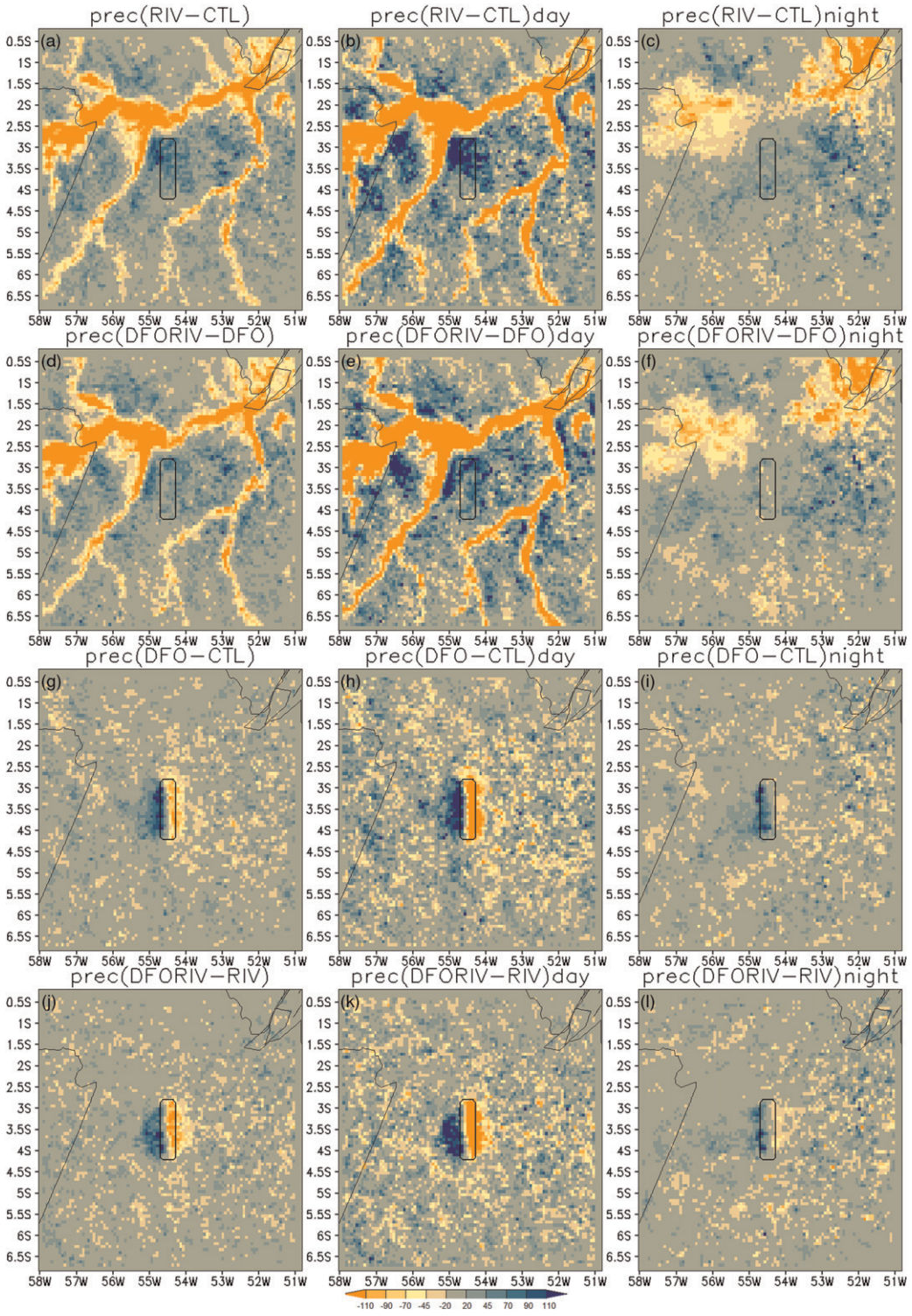

Figure 18. Mean difference of precipitation (mm month^{-1}) for the experiments (a)–(c) RIV − CTL, (d)–(f) DFORIV − DFO, (g)–(i) DFO − CTL, and (j)–(l) DFORIV − RIV. Shown are (left) daily precipitation, (middle) daytime precipitation only, and (right) the nocturnal precipitation only. The rectangle shows the cleared area.

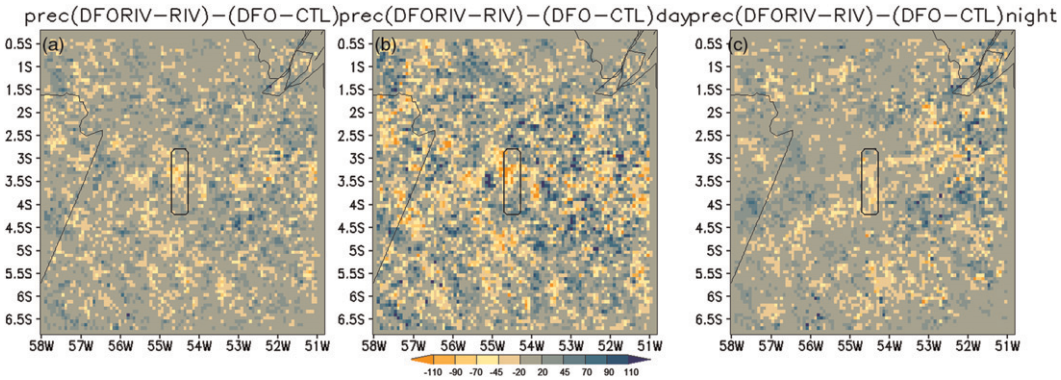

Figure 19. Mean difference of precipitation (mm month^{-1}) of the experiments (DFORIV − RIV) − (DFO − CTL) during (a) 24 h, (b) the daytime only, and (c) the nighttime only.

the area and shape of deforestation and the soil moisture status influenced the state of the atmosphere during the time scale of several weeks, with distinguishable patterns of temperature, humidity, and rainfall. Deforestation resulted in an increase in the Bowen ratio and in the development of a three-dimensional thermal cell slightly shifted downwind from the large-scale circulation. The deforestation breeze increased rainfall near the downwind edge of the clearance and decreased it near the upwind edge. In addition, the boundary layer was warmer and drier above 1000-m height and was slightly wetter up to 2000-m height. More precisely, certain variables were apparently necessary to strengthen the modeled deforestation breeze and control the impacts on rainfall, namely,

(i) soil moisture status: this affected the circulation energetics proportionally to the soil dryness, especially for soil wetness conditions below ~0.6; on the other hand, rainfall decreased proportionally to the soil moisture wetness, above the ~0.6) threshold;
(ii) patch shape of deforestation: the horizontal strips lined up with the prevailing wind showed a dominant increase in rainfall over the deforestation, an effect that was apparently less influential in the larger patches; with the patches aligned in the opposite direction (north–south), the sectors with either increase or decrease in precipitation appeared to be in two quite distinct positions, as a result of two upward and clearly separated downward branches.

Our modeling investigation drew heavily upon simple hypothesis, necessary to make the study feasible, which notwithstanding brought interesting results to understand the broader impacts of tropical deforestation. It also includes the study of processes and phenomena that require more clarification. We relied on the model performance for cloud cover and radiation parameterization, which needs refinement to compare ground data with greater accuracy. The shape of the deforestation patches were also too simplified, which is not realistic in the current land use of the region under study. Amazonian deforestation is more often a mosaic of forest and pasturelands, which also includes croplands in some areas (e.g., southern Amazonia). A realistic representation of the land-use changes

requires a very fine modeled resolution in the scale below 1 km; appropriate parameterization of boundary layer turbulent processes and cloud development; and powerful computation to enable various cases of seasonal, intraseasonal, and interannual climate variability.

We believe the question of rainfall changes in Amazonian deforestation remains open. Previous observational and mesoscale modeling studies of Amazonian deforestation did not form a consensus, and neither did they fully agree with the results of large-scale models. Our results indicate possible values for the area size threshold above which rainfall decreases with deforestation as indicated by large-scale models. For the north–south-oriented patches, it is seen that the change from increased to decreased rainfall occurs for an area of 15 000 km^2; for the tilted patches, this threshold is about 50 000 km^2 for the rainy season and 60 000 km^2 for the dry season. The implications of these values on the possible overall effect of actual deforestation patches in the Amazon and on overall rainfall is an issue that should be further investigated, including both suggestions to focus modeling strategies and strategies to collect field observational data to survey the regions with land-use change.

Acknowledgments. The authors thank Fundação de Amparo à Pesquisa do Estado de São Paulo (FAPESP; Projects 05/57829-0, 02/09289-9, and 08/58120-3). The first author would like to thank Jonathan Mota da Silva, Marcos Oyama, and Leila Maria Vespoli de Carvalho for valuable suggestions.

References

Avissar, R., and D. Werth, 2005: Global hydroclimatological teleconnections resulting from tropical deforestation. *J. Hydrometeor.,* **6,** 134–145.

——, P. L. Silva Dias, M. A. F. Silva Dias, and C. Nobre, 2002: The Large-Scale Biosphere-Atmosphere Experiment in Amazonia (LBA): Insights and future research needs. *J. Geophys. Res.,* **107,** 8086, doi:10.1029/2002JD002704.

Baidya Roy, S., and R. Avissar, 2002: Impact of land use/land cover change on regional hydrometeorology in Amazonia. *J. Geophys. Res.,* **107,** 8037, doi:10.1029/2000JD000266.

Betts, A. K., and M. A. F. Silva Dias, 2010: Progress in understanding land–surface–atmosphere coupling from LBA research. *J. Adv. Model. Earth Syst.,* **2,** doi:10.3894/JAMES.2010.2.6.

Bruno, R. D., H. R. da Rocha, H. C. de Freitas, M. L. Goulden, and S. D. Miller, 2006: Soil moisture dynamics in an eastern Amazonian tropical forest. *Hydrol. Proc.,* **20,** 2477–2489.

Chen, C., and W. R. Cotton, 1983: A one-dimensional simulation of the strato-cumulus-capped mixed layer. *Bound.-Layer Meteor.,* **25,** 289–381.

Cotton, W. R., and Coauthors, 2003: RAMS 2001: Current status and future directions. *Meteor. Atmos. Phys.,* **82** (1–4), 5–29.

Cutrim, E., D. W. Martin, and R. Rabin, 1995: Enhancement of cumulus clouds over deforested lands in Amazonia. *Bull. Amer. Meteor. Soc.,* **76,** 1801–1805.

D'Almeida, C., C. J. Vörösmarty, G. C. Hurtt, J. A. Marengo, S. L. Dingman, and B. D. Keim, 2007: The effects of deforestation on the hydrological cycle in Amazonia: A review on scale and resolution. *Int. J. Climatol.,* **27,** 633–647.

da Rocha, H. R., C. A. Nobre, J. Bonatti, I. R. Wright, and P. J. Sellers, 1996: A vegetation-atmosphere interaction study for Amazonian deforestation using field data and a single column model. *Quart. J. Roy. Meteor. Soc.,* **122,** 567–594.

——, M. L. Goulden, S. D. Miller, M. C. Menton, L. D. V. O. Pinto, H. C. Freitas, and A. M. S. Figueira, 2004: Seasonality of water and heat fluxes over a tropical forest in eastern Amazonia. *Ecol. Appl.,* **14,** S22–S32.

——, and Coauthors, 2009a: Patterns of water and heat flux across a biome gradient from tropical forest to savanna in Brazil. *J. Geophys. Res.,* **114,** G00B12, doi:10.1029/2007JG000640.

——, A. Manzi, and W. Shuttleworth, 2009b: Evapotranspiration. *Amazonia and Global Change, Geophys. Monogr.,* Vol. 126, Amer. Geophys. Union, 261–272.

Findell, K. L., T. R. Knutson, and P. C. D. Milly, 2006: Weak simulated extratropical responses to complete tropical deforestation. *J. Climate,* **19,** 2835–2850.

Fisch, G., J. Tota, L. A. Machado, M. A. F. Silva Dias, R. F. F. Lyra, C. Nobre, A. Dolman, and J. H. C. Gash, 2004: The convective boundary layer over pasture and forest in Amazonia. *Theor. Appl. Climatol.,* **78** (1–3), 47–59.

Fitzjarrald, D. R., R. K. Sakai, O. L. L. Moraes, R. Cosme de Oliveira, O. C. Acevedo, M. J. Czikowsky, and T. Beldini, 2008: Spatial and temporal rainfall variability near the Amazon-Tapajós confluence. *J. Geophys. Res.,* **113,** G00B11, doi:10.1029/2007JG000596.

Freitas, S. R., and Coauthors, 2009: The Coupled Aerosol and Tracer Transport model to the Brazilian developments on the Regional Atmospheric Modeling System (CATT-BRAMS)—Part 1: Model description and evaluation. *Atmos. Chem. Phys.,* **9,** 2843–2861.

Gandu, A. W., J. C. P. Cohen, and J. R. S. de Souza, 2004: Simulation of deforestation in eastern Amazonia using a high-resolution model. *Theor. Appl. Climatol.,* **78** (1–3), 123–135.

Gash, J. H. C., C. A. Nobre, J. M. Roberts, and R. L. Victoria, 1996: *Amazonian Deforestation and Climate*. John Wiley, 611 pp.

Grell, G. A., and D. Dévényi, 2002: A generalized approach to parameterizing convection combining ensemble and data assimilation techniques. *Geophys. Res. Lett.,* **29,** 1693, doi:10.1029/2002GL015311.

Hutyra, L. R., J. W. Munger, C. A. Nobre, S. R. Saleska, S. A. Vieira, and S. C. Wofsy, 2005: Climatic variability and vegetation vulnerability in Amazônia. *Geophys. Res. Lett.,* **32,** L24712, doi:10.1029/2005GL024981.

Martins, J. A., M. A. F. Silva Dias, and F. L. T. Gonçalves, 2009: Impact of biomass burning aerosols on precipitation in the Amazon: A modeling case study. *J. Geophys. Res.,* **114,** D02207, doi:10.1029/2007JD009587.

Negri, A. J., R. F. Adler, L. Xu, and J. Surrat, 2004: The impact of Amazonian deforestation on dry season rainfall. *J. Climate,* **17,** 1306–1319.

Nepstad, D. C., C. M. Stickler, B. Soares-Filho, and F. Merry, 2008: Interactions among Amazon land use, forests and climate: Prospects for a near-term forest tipping point. *Philos. Trans. Roy. Soc. London,* **363B,** 1737–1746.

Nobre, C. A., P. J. Sellers, and J. Shukla, 1991: Amazonian deforestation and regional climate change. *J. Climate,* **4,** 957–988.

——, G. Fisch, H. R. Rocha, R. F. F. Lyra, E. J. P. Rocha, A. C. L. da Costa, and V. N. Ubarana, 1996: Observations of the atmospheric boundary layer in Rondonia. *Amazonia Deforestation and Climate,* J. H. C. Gash et al., Eds., John Wiley & Sons, 425–435.

Oyama, M. D., and C. A. Nobre, 2003: A new climate-vegetation equilibrium state for tropical South America. *Geophys. Res. Lett.,* **30,** 2199–2203.

Pielke, R. A., 2002: Model evaluation. *Mesoscale Meteorological Modeling,* R. Dmowska, J. R. Holton, and H. T. Rossby, Eds., Academic Press, 442–471.

——, and Coauthors, 1992: A comprehensive meteorological modeling system—RAMS. *Meteor. Atmos. Phys.,* **49** (1–4), 69–91.

Ramos da Silva, R., D. Werth, and R. Avissar, 2008: Regional impacts of future land-cover changes on the Amazon basin wet-season climate. *J. Climate,* **21,** 1153–1170.

Sakai, R. K., and Coauthors, 2004: Land-use change effects on local energy, water, and carbon balances in an Amazonian agricultural field. *Global Change Biol.,* **10,** 895–907.

Sampaio, G., C. Nobre, M. H. Costa, P. Satyamurty, B. S. Soares-Filho, and M. Cardoso, 2007: Regional climate change over eastern Amazonia caused by pasture and soybean cropland expansion. *Geophys. Res. Lett.,* **34,** LI7709, doi:10.1029/2007GL030612.

Segal, M., R. Avissar, M. C. McCumber, and R. A. Pielke, 1988: Evaluation of vegetation effects on the generation and modification of mesoscale circulations. *J. Atmos. Sci.,* **45,** 2268–2292.

Silva Dias, M. A. F., P. L. Silva Dias, M. Longo, D. R. Fitzjarrald, and A. S. Denning, 2004: River breeze circulation in eastern Amazonia: Observations and modelling results. *Theor. Appl. Climatol.,* **78** (1–3), 111–121.

Walko, R. L., and Coauthors, 2000: Coupled atmosphere–biophysics–hydrology models for environmental modeling. *J. Appl. Meteor.,* **39,** 931–944.

Wang, J., and Coauthors, 2009: Impact of deforestation in the Amazon basin on cloud climatology. *Proc. Natl. Acad. Sci. USA,* **106,** 3670–3674.

Werth, D., and R. Avissar, 2002: The local and global effects of Amazon deforestation. *J. Geophys. Res.,* **107,** 8087, doi:10.1029/2001JD000717.